Atomic-Resolution Three-Dimensional Structure of HET-s(218-289) Amyloid Fibrils by Solid-State NMR Spectroscopy

ARTICLE *in* JOURNAL OF THE AMERICAN CHEMICAL SOCIETY · OCTOBER 2010

Impact Factor: 12.11 · DOI: 10.1021/ja104213j · Source: PubMed

7 AUTHORS, INCLUDING:

Christian Wasmer
Harvard Medical School
18 PUBLICATIONS **1,165** CITATIONS
SEE PROFILE

Eiso Ab
Leiden University
27 PUBLICATIONS **858** CITATIONS
SEE PROFILE

Anja Böckmann
University of Lyon
92 PUBLICATIONS **2,550** CITATIONS
SEE PROFILE

Beat H Meier
ETH Zurich
269 PUBLICATIONS **13,517** CITATIONS
SEE PROFILE

J|A|C|S
ARTICLES

Atomic-Resolution Three-Dimensional Structure of HET-s(218−289) Amyloid Fibrils by Solid-State NMR Spectroscopy

Hélène Van Melckebeke,[†] Christian Wasmer,[†] Adam Lange,[†,||] Eiso AB,[§] Antoine Loquet,[‡,||] Anja Böckmann,[‡] and Beat H. Meier*[,†]

Physical Chemistry, ETH Zürich, Wolfgang-Pauli-Strasse 10, CH-8093 Zurich, Switzerland, Institut de Biologie et Chimie des Protéines, UMR 5086 CNRS/Université de Lyon 1, 7 passage du Vercors, 69367 Lyon, France, and ZoBio BV, Einsteinweg 55, 2333 CC Leiden, The Netherlands

Received May 16, 2010; E-mail: beme@ethz.ch

Abstract: We present a strategy to solve the high-resolution structure of amyloid fibrils by solid-state NMR and use it to determine the atomic-resolution structure of the prion domain of the fungal prion HET-s in its amyloid form. On the basis of 134 unambiguous distance restraints, we recently showed that HET-s(218−289) in its fibrillar state forms a left-handed β-solenoid, and an atomic-resolution NMR structure of the triangular core was determined from unambiguous restraints only. In this paper, we go considerably further and present a comprehensive protocol using six differently labeled samples, a collection of optimized solid-state NMR experiments, and adapted structure calculation protocols. The high-resolution structure obtained includes the less ordered but biologically important C-terminal part and improves the overall accuracy by including a large number of ambiguous distance restraints.

Introduction

Filamentous proteins are used by nature for many functions but are also linked to important diseases such as Alzheimer's disease, where the appearance of neurofibrillar tangles and amyloid plaques are important elements of the pathology,[1] and the transmissible prion encephalopathies. The proteins that appear in these deposits can also be aggregated in vitro where they typically form fibrils.[2] Most of these fibrils are amyloids, and the formation of a cross-β-backbone[3] is the central element of this type of fibril assembly. The three-dimensional (3D) structure of most protein fibrils is not known to atomic resolution, despite their biological significance, in particular for prions, where the 3D structure is thought to be the sole difference between the normal and the alternatively folded ("diseased") form of the protein.[4] Indeed, being neither 2D nor 3D-crystalline nor soluble, protein fibrils are difficult to investigate by X-ray diffraction or solution NMR methods, and the application of solid-state NMR is the method of choice for the characterization of their structure and dynamics.[5,6] NMR is particularly useful for fibrils that are highly ordered on a local scale and consequently show NMR resonance lines as narrow as the ones in typical microcrystalline preparations.[7−13]

The structure of the HET-s prion domain HET-s(218−289) (PDB code: 2RNM) was recently determined based on spectrally unambiguous NMR distance restraints.[14] HET-s is a protein of the filamentous fungus *Podospora anserina* which can exist in two conformations: a fibrillar form which was characterized previously as an amyloid,[7,11] and a soluble form in which most of the C-terminal prion domain (residues 218−289) is unstructured while residues 1−227 form a compact and well-defined fold.[15] In its prion form, HET-s plays a role in heterokaryon incompatibility, a fungal self/nonself recognition phenomenon that may prevent different forms of parasitism. It represents an ideal model system for the study of prions, it can easily be

[†] ETH Zürich.
[‡] UMR 5086 CNRS/Université de Lyon 1.
[§] ZoBio BV.
[||] Current address: Max Planck Institute for Biophysical Chemistry, Am Fassberg 11, 37077 Göttingen, Germany.

(1) Duyckaerts, C.; Delatour, B.; Potier, M.-C. *Acta Neuropathol.* **2009**, *118*, 5.
(2) Chiti, F.; Dobson, C. M. *Annu. Rev. Biochem.* **2006**, *75*, 333.
(3) Hennetin, J.; Jullian, B.; Steven, A. C.; Kajava, A. V. *J. Mol. Biol.* **2006**, *358*, 1094.
(4) Prusiner, S. B. *Science* **1982**, *216*, 136.
(5) Böckmann, A. *Angew. Chem., Int. Ed.* **2008**, *47*, 6110.
(6) Böckmann, A.; Meier, B. H. *Prion* **2010**, *4*, 1.
(7) Wasmer, C.; Schütz, A.; Loquet, A.; Buhtz, C.; Greenwald, J.; Riek, R.; Böckmann, A.; Meier, B. *J. Mol. Biol.* **2009**, *394*, 119.
(8) Loquet, A.; Bousset, L.; Gardiennet, C.; Sourigues, Y.; Wasmer, C.; Habenstein, B.; Schütz, A.; Meier, B.; Melki, R.; Böckmann, A. *J. Mol. Biol.* **2009**, *394*, 108.
(9) Siemer, A. B.; Ritter, C.; Steinmetz, M. O.; Ernst, M.; Riek, R.; Meier, B. H. *J. Biomol. NMR* **2006**, *34*, 75.
(10) Siemer, A. B.; Ritter, C.; Ernst, M.; Riek, R.; Meier, B. H. *Angew. Chem., Int. Ed.* **2005**, *44*, 2441.
(11) Ritter, C.; Maddelein, M. L.; Siemer, A. B.; Luhrs, T.; Ernst, M.; Meier, B. H.; Saupe, S. J.; Riek, R. *Nature* **2005**, *435*, 844.
(12) Heise, H.; Hoyer, W.; Becker, S.; Andronesi, O. C.; Riedel, D.; Baldus, M. *Proc. Natl. Acad. Sci. U.S.A.* **2005**, *102*, 15871.
(13) Helmus, J. J.; Surewicz, K.; Nadaud, P. S.; Surewicz, W.; Jaroniec, C. P. *Proc. Natl. Acad. Sci. U.S.A.* **2008**, *105*, 6284.
(14) Wasmer, C.; Lange, A.; van Melckebeke, H.; Siemer, A. B.; Riek, R.; Meier, B. H. *Science* **2008**, *319*, 1523.
(15) Balguerie, A.; Dos Reis, S.; Ritter, C.; Chaignepain, S.; Coulary-Salin, B.; Forge, V.; Bathany, K.; Lascu, I.; Schmitter, J.; Riek, R.; Saupe, S. J. *EMBO J.* **2003**, *22*, 2071.

produced, and the fibrils can reproducibly be prepared in always the same conformer.

We here extend our initial structural analysis[14] of HET-s(218−289) which was based on 134 unambiguous distant restraints and show how a large number (over 2500) of intra- and intermolecular restraints can be obtained for these fibrils, which types of restrains are essential, and how the many ambiguous restraints can be used in a protocol to calculate the fibril structure. In particular, symmetry considerations, the calibration of the distance restraints, and the structural content of different types of spectra are discussed. The proposed protocol allows one to obtain a highly resolved 3D structure of HET-s(218−289) in its amyloid form and should be applicable to other amyloids as well.

Protocol for Structure Determination and Results

Sequential Resonance Assignments. From solid-state NMR spectra of HET-s(218−289), obtained using cross-polarization as the initial transfer step, we have sequentially assigned signals for 56 out of 71 residues (I222-A249, T260-W287, see Figure S1 in the Supporting Information for the amino acid sequence). Compared to previously published data[9−11,14,16] (BMRB ID 11028), the assignment of HET-s(218−289) has been extended and was deposited in the BMRB under the accession code 11064. The newly assigned residues I222-R225, A249, and G283-G285 are located at the edge of the rigid core of the fibrils[14] and mainly correspond to weaker signals which had not been detected in the previous experiments.

Packing and Symmetry. In amyloids, β-strands from different protein molecules form a continuous, extended β-sheet perpendicular to the fibril axis.[17,18] This arrangement induces close proximity of both backbone and side-chain atoms of neighboring molecules. The intermolecular contacts are therefore expected to be numerous and intense, as structurally meaningful $^{13}C-^{13}C$ or $^{1}H-^{1}H$ inter- and intramolecular distances are similar. Therefore, experiments that adequately measure both, and distinguish between, *intra*molecular and *inter*molecular distances are needed. If several protofilaments arrange in a regular manner to form thicker fibrils, it could also be possible to observe contacts between protofilaments. An obvious and successful way of discriminating between intra- and intermolecular contacts is to use mixtures of differentially labeled protein monomers.[19,20] Note that, for crystalline proteins, intermolecular restraints were mainly disregarded for structure determination so far[21−26] because the high water content of most protein crystals makes short intermolecular contacts much less abundant than for fibrils.

The possible packing schemes for fibrillar proteins are numerous and range from quasi-one-dimensional systems where a single molecule is repeated along the fibril axis and where a given protein has contact with two other protein molecules ("above" and "below") only[7,11] (Figure 1), to assemblies of a few molecules in the transverse plane,[18,27−29] to superhelical arrangements of molecules,[8,30−32] to three-dimensional objects with six or more close neighbors in space.[33]

In the following, we focus on the simplest amyloid fibrils, which form a spine of β-sheets with a mass-per-length (MPL) ratio corresponding to one molecule per length of the unit cell along the fibril axis (Figure 1). The geometry of the cross-β-sheets is governed by the formation of a large number of hydrogen bonds roughly parallel to the fiber axis, and the formation of the fibril can be envisioned as the stacking of cuboids (see Figure 1). Such systems can be classified as β-solenoids.[31,34] One molecule can form one or several turns of the solenoid. In the simplest case, there is only one asymmetric unit in the unit cell: the fibril consists of a single molecule, repeated thousands of times along the fiber axis which we assume to be a straight line (Figure 1a). Structurally identical molecules are then connected by a screw axis. The symmetry group is $p11N_1$, where $\alpha = 2\pi/N$ gives the twist angle along the fibril axis, which we denote as the z direction. To ensure the formation of an extended H-bond network, α is restricted to a few degrees. This symmetry describes parallel in-register β-sheets, which have been detected for many amyloids, in particular those formed by proteins with several β-strands.[35−37] In this model, all intermolecular interfaces are identical. A slightly more complex stacking arises if two consecutive blocks involve a further π rotation, around the x-, y-, or z-axis (Figure 1b and c). Note that x or y rotations (rotation axis orthogonal to the fibril direction) both lead to an antiparallel intermolecular β-sheet. In this case, the repeating units consist of two molecules. This arrangement defines two different types of molecular interfaces, which alternate along the fibril axis. All these models show a mass-per-length ratio of one (in units of molecules divided by the length of the unit cell along the fibril dimension), which is experimentally accessible, for example, by scanning transmission electron microscopy (STEM) mea-

(16) Siemer, A. B.; Arnold, A. A.; Ritter, C.; Westfeld, T.; Ernst, M.; Riek, R.; Meier, B. H. *J. Am. Chem. Soc.* **2006**, *128*, 13224.
(17) Sawaya, M. R.; Sambashivan, S.; Nelson, R.; Ivanova, M. I.; Sievers, S. A.; Apostol, M. I.; Thompson, M. J.; Balbirnie, M.; Wiltzius, J. J. W.; McFarlane, H. T.; Madsen, A. O.; Riekel, C.; Eisenberg, D. *Nature* **2007**, *447*, 453.
(18) Nelson, R.; Sawaya, M. R.; Balbirnie, M.; Madsen, A. O.; Riekel, C.; Grothe, R.; Eisenberg, D. *Nature* **2005**, *435*, 773.
(19) Etzkorn, M.; Böckmann, A.; Lange, A.; Baldus, M. *J. Am. Chem. Soc.* **2004**, *126*, 14746.
(20) Lange, A.; Meier, B. H. *C. R. Chim.* **2008**, *11*, 332.
(21) Castellani, F.; van Rossum, B.; Diehl, A.; Schubert, M.; Rehbein, K.; Oschkinat, H. *Nature* **2002**, *420*, 98.
(22) Zech, S. G.; Wand, A. J.; McDermott, A. E. *J. Am. Chem. Soc.* **2005**, *127*, 8618.
(23) Lange, A.; Giller, K.; Hornig, S.; Martin-Eauclaire, M. F.; Pongs, O.; Becker, S.; Baldus, M. *Nature* **2006**, *440*, 959.
(24) Franks, W. T.; Wylie, B. J.; Frericks Schmidt, H. L.; Nieuwkoop, A. J.; Mayrhofer, R.; Shah, G. J.; Graesser, D. T.; Rienstra, C. M. *Proc. Natl. Acad. Sci. U.S.A.* **2008**, *105*, 4621.
(25) Loquet, A.; Bardiaux, B.; Gardiennet, C.; Blanchet, C.; Baldus, M.; Nilges, M.; Malliavin, T.; Böckmann, A. *J. Am. Chem. Soc.* **2008**, *130*, 3579.
(26) Manolikas, T.; Herrmann, T.; Meier, B. H. *J. Am. Chem. Soc.* **2008**, *130*, 3959.
(27) Paravastu, A. K.; Leapman, R. D.; Yau, W.; Tycko, R. *Proc. Natl. Acad. Sci. U.S.A.* **2008**, *105*, 18349.
(28) Tycko, R. *Q. Rev. Biophys.* **2006**, *39*, 1.
(29) Nielsen, J.; Bjerring, M.; Jeppesen, M.; Pedersen, R.; Pedersen, J.; Hein, K.; Vosegaard, T.; Skrydstrup, T.; Otzen, D.; Nielsen, N. *Angew. Chem., Int. Ed.* **2009**, *48*, 2118.
(30) Li, H.; DeRosier, D. J.; Nicholson, W. V.; Nogales, E.; Downing, K. H. *Structure* **2002**, *10*, 1317.
(31) Kajava, A. V.; Squire, J. M.; Parry, D. A. D. *Adv. Protein Chem.* **2006**, *73*, 1.
(32) Kajava, A. V.; Baxa, U.; Wickner, R. B.; Steven, A. C. *Proc. Natl. Acad. Sci. U.S.A.* **2004**, *101*, 7885.
(33) Steinmetz, M.; Gattin, Z.; Verel, R.; Ciani, B.; Stromer, T.; Green, J. M.; Tittmann, P.; Schulze-Briese, C.; Gross, H.; van Gunsteren, W. F.; Meier, B. H.; Serpell, L. C.; Muller, S. A.; Kammerer, R. A. *J. Mol. Biol.* **2008**, *376*, 898.
(34) Kajava, A. V.; Squire, J. M.; Parry, D. A. *Adv. Protein Chem.* **2006**, *73*, 55.
(35) Shewmaker, F.; Wickner, R. B.; Tycko, R. *Proc. Natl. Acad. Sci. U.S.A.* **2006**, *103*, 19754.
(36) Wickner, R.; Shewmaker, F.; Kryndushkin, D.; Edskes, H. *BioEssays* **2008**, *30*, 955.
(37) Shewmaker, F.; Ross, E. D.; Tycko, R.; Wickner, R. B. *Biochemistry* **2008**, *47*, 4000.

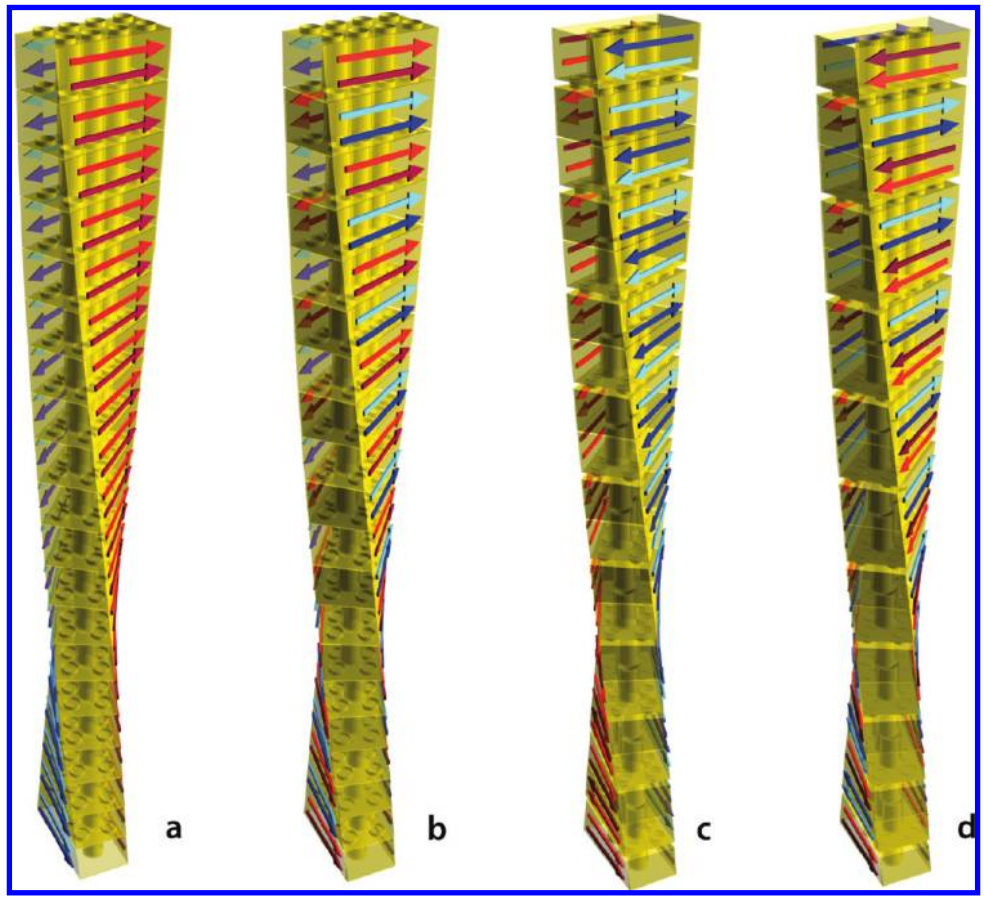

Figure 1. Stacking models for cross-β-fibrils. In the figure, a molecule with two turns per molecule (two layers of β-strands) is depicted, corresponding to the conformation already identified early on for HET-s(218−289).[11] For the parallel in register models (a) and (b), one molecule forms a unit cell, symbolized by a single Duplo block. Note that the top and bottom surfaces are twisted here as an example by an angle $\alpha = 4°$. In (b), an additional 180° rotation around the fibril axis is added. For the antiparallel arrangements in (c) and (d), half of the Duplo blocks are rotated by a 180° rotation around either the *x*- or the *y*-axis (perpendicular to the fiber axis). This antiparallel arrangement defines two different types of molecular interfaces, which alternate along the fibril axis. The examples shown do not include a register shift, which may be added.

surements, and contain symmetry-equivalent proteins, which predicts a single set of solid-state NMR resonances. Both of these properties were confirmed for the HET-s(218−289) system.[9,38] The absence of any peak doublings in the NMR spectra is a strong indication that all molecules are symmetry related as discussed above, as chemical shifts are highly sensitive to the polypeptide conformation. In both models, different registers are possible including out-of-register parallel and antiparallel β-sheets.

Implementation of Symmetry Restraints. We have used CYANA[39] to determine the HET-s(218−289) fibril structure. Because crystallographic symmetry of the type described above is not implemented in CYANA 2, we calculated a segment of the fibrils containing several molecules (between 2 and 9) and implemented the symmetry of the fibril by introducing quadratic pseudoenergy terms that request all molecules to have very similarly structured rigid parts (residues I222−L251 and T260−W287) and also request translational symmetry. We use both angular restraints ensuring that the Φ and Ψ backbone dihedral angles are similar in all molecules (in analogy to the noncrystallographic symmetry of CNS[40]) and distance restraints requesting that the intermolecular distances between the same atoms in molecules j and $j + 1$ are identical for all j (as also used in ref 41). In fact, the symmetry restraints are less stringent than the symmetry imposed in Figure 1 and allow for arbitrary twist and tilt angles, as well as register shifts.

NMR Distance Restraints. NMR experiments were recorded on samples with three complementary kinds of labeling schemes, from which three different types of restraints were deduced: (i) Ambiguous intra/intermolecular restraints were extracted from "homogeneous" samples, containing molecules all labeled the same way, namely, uniformly $^{13}C-^{15}N$ fully labeled or "checkerboard labeled" samples.[21,42] (ii) Unambiguously intramolecular restraints were extracted from so-called "diluted" samples, for which unlabeled and labeled protein monomers are mixed before fibrillization at a ratio of 2.5:1. (iii) Unambiguously intermolecular restraints were extracted from so-called "mixed" samples produced from ^{15}N and ^{13}C labeled monomers that were mixed before fibrillization at a 1:1 ratio. A full list of the samples used and the extracted restraints is given Table 1.

The implementation of the distance restraints in the structure calculation for each kind of sample is summarized in Figure 2

(38) Sen, A.; Baxa, U.; Simon, M. N.; Wall, J. S.; Sabate, R.; Saupe, S. J.; Steven, A. C. *J. Biol. Chem.* **2007**, *282*, 5545.
(39) Guntert, P.; Mumenthaler, C.; Wuthrich, K. *J. Mol. Biol.* **1997**, *273*, 283.
(40) Brünger, A. T.; Adams, P. D.; Clore, G. M.; DeLano, W. L.; Gros, P.; Grosse-Kunstleve, R. W.; Jiang, J. S.; Kuszewski, J.; Nilges, M.; Pannu, N. S.; Read, R. J.; Rice, L. M.; Simonson, T.; Warren, G. L. *Acta Crystallogr., Sect. D: Biol. Crystallogr.* **1998**, *54*, 905.
(41) Nilges, M. *Proteins* **1993**, *17*, 297.
(42) LeMaster, D. M.; Cronan, J. E. *J. Biol. Chem.* **1982**, *257*, 1224.

Table 1. Statistics about the Peaks Picked in Spectra Used for the Definition of Upper Limit Distance Restraints and Other Restraints Used for the Structure Calculation, Given per Molecule

					no. of ambiguities (per peak)[d]	
sample type	labeling and spectrum type	no. of picked peaks (intrares.)[a,b]	tolerance (ppm)[c]	upper-limit distance (Å)[b]	first calc.	last calc.
diluted	2-^{13}C PDSD	197	0.3	CC	2155	532
		(+192)		6.5	(10.9)	(2.7)
	1,3-^{13}C PDSD	199	0.3	CC	2363	647
		(+245)		7.0	(11.9)	(3.3)
	U-^{13}C^{15} N CHHC	350	0.3	HH	5177	1077
		182/168		3.5/4.5	(14.8)	(3.1)
mixed	^{15}N/^{13}C NHHC	24	0.5/1.0	HH	922 × 2	71
		15/9		3.5/4.5	(38.4 × 2)	(3.0)
	^{15}N/^{13}C PAIN	114	0.4/0.8	NC	1993 × 2	391
		21/9		35.0/7.0	(17.5 × 2)	(3.4)
homogeneous	2-^{13}C PDSD	811	0.3	CC	8144 × 3	4643
		(+385)		8.0	(10.0 × 3)	(5.7)
	U-^{13}C^{15}N PAR	231 (+309)	0.3	CC	2172 × 3	1068
		99/147		6.0/7.0	(9.4 × 3)	(4.6)
	U-^{13}C^{15}N NHHC	201	0.3/0.6	HH	2183 × 3	534
		80/121		3.5/4.5	(10.9 × 3)	(2.7)
	U-^{13}C^{15}N CHHC	504	0.3	HH	4429 × 3	2064
		233/271		3.5/5.0	(8.8 × 3)	(4.1)
total		2631			66 309	11 027
		(+1131)			(25.2)	(4.2)
TALOS		82				
symmetry		all assigned residues (I222−A249,T260−W287)				
H-bonds		23 (12 intra, 11 inter)				

[a] The first number gives the total number of picked peaks used for the structure calculations. For the PDSD and PAR spectra, peaks corresponding to intraresidue correlations were excluded from the structure calculations and are not taken into account for the statistics about ambiguities. Their numbers are given in parentheses. [b] For the CHHC, NHHC, and PAIN spectra, the peaks were separated into two classes according to their intensities. The parameters and statistics for both intensity classes are given on the second line of the cell (high intensity/low intensity). [c] The two values correspond to the tolerances used for the ^{13}C and ^{15}N dimensions, respectively. [d] The number of ambiguities is given per molecule and for all restraints used for the structure calculation (and the average per restraint in parentheses). For the first round of calculations, this number is equal to the spectral ambiguities for the given tolerance multiplied by two or three for the spectra recorded on mixed or homogeneous samples, respectively, in order to take into account the intraintermolecular ambiguities. For the final calculation, some of the initial ambiguities were discarded by comparison to the structures obtained in the first round as described in the main text.

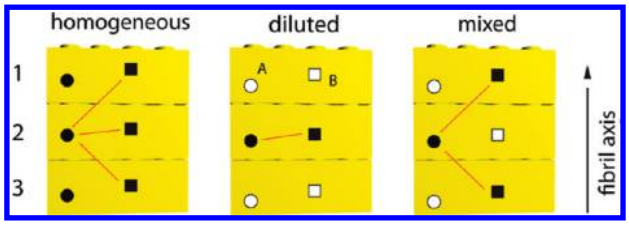

Figure 2. Schematic representation of the implementation of upper-limit distance restraints. On each of the three consecutive molecules (here depicted like Figure 1a, but applicable for all other models as well), two atoms A and B are shown as a circle and a square, respectively. Filled symbols represent labeled atoms (^{15}N and ^{13}C), and open symbols unlabeled atoms. The red lines show, on the example of atom A2, the different restraint assignment possibilities. For homogeneous labeling, A2-B restraints can be assigned to three possible distances, while two (intermolecular) possibilities exist, for mixed samples and only one (intramolecular) for diluted samples.

for three molecules that are representative for all models of Figure 1. In homogeneous samples, each cross peak between nuclei A and B is interpreted as two ambiguous restraints starting at the central molecule with three assignment possibilities each, for example: {A2-B2, A2-B1, or A2-B3} (as indicated by lines in Figure 2) and {A2-B2, A1-B2, or A3-B2}. In diluted samples, the distance restraints extracted from the experiments were unambiguously used as intramolecular restraints ({A2-B2}). For mixed samples, one cross peak in the spectrum gives rise to two restraints with two assignment possibilities each, {A2-B1 or A2-B3} and {A1-B2 or A3-B2}. Note that such an implementation does not discriminate a priori between the different models of Figure 1.

The experiments performed on the three samples are listed in Table 1. Representative examples of the different types of spectra are shown in Figure 3. It should be noted that all the experiments performed for distance measurements rely on second-order terms that are caused by cross-terms between two different interactions[43−46] involving three spins. Nevertheless, as a workable approximation,[26] the cross-peak intensities extracted from the 2D spectra are interpreted in terms of distances between the two spins resonating at the respective frequencies. Distances from ^{13}C-detected proton spin-diffusion CHHC and NHHC experiments[47,48] were interpreted as proton−proton distances, whereas distance restraints extracted from proton-driven ^{13}C spin-diffusion (PDSD)[43,49,50] and PAR[45] experiments

(43) Grommek, A.; Meier, B. H.; Ernst, M. *Chem. Phys. Lett.* **2006**, *427*, 404.
(44) Scholz, I.; Meier, B. H.; Ernst, M. *J. Chem. Phys.* **2007**, *127*, 204504.
(45) De Paëpe, G.; Lewandowski, J. R.; Loquet, A.; Böckmann, A.; Griffin, R. G. *J. Chem. Phys.* **2008**, *129*, 245101.
(46) Lewandowski, J. R.; De Paepe, G.; Griffin, R. G. *J. Am. Chem. Soc.* **2007**, *129*, 728.
(47) Lange, A.; Luca, S.; Baldus, M. *J. Am. Chem. Soc.* **2002**, *124*, 9704.
(48) Lange, A.; Becker, S.; Seidel, K.; Giller, K.; Pongs, O.; Baldus, M. *Angew. Chem., Int. Ed.* **2005**, *44*, 2089.

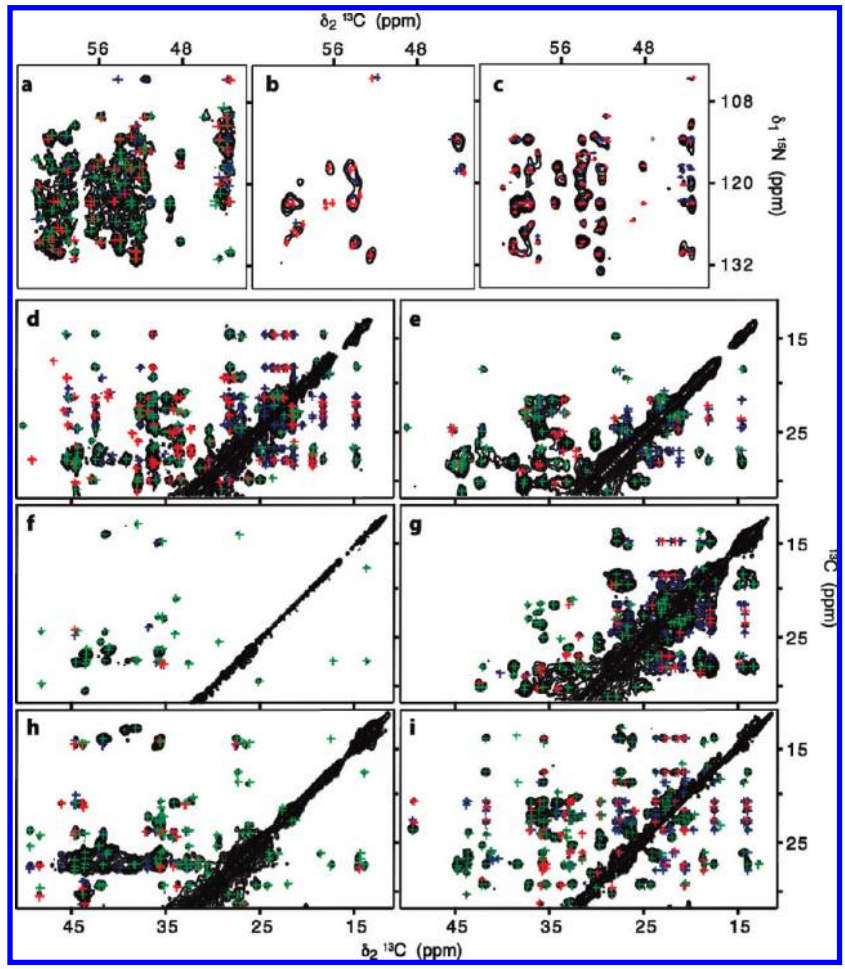

Figure 3. Extracts from spectra recorded on the different samples. (a) NHHC, recorded on a uniformly $^{13}C-^{15}N$ labeled sample; (b) NHHC and (c) PAIN spectra recorded on $^{13}C/^{15}N$ mixed samples; (d) CHHC, recorded on a uniformly $^{13}C-^{15}N$ labeled sample; (e) CHHC, recorded on a diluted, uniformly $^{13}C-^{15}N$ labeled sample; (f) PDSD, recorded on a diluted 2-^{13}C-glycerol-grown checkerboard sample; (g) PDSD, recorded on a diluted 1,3-^{13}C-glycerol-grown checkerboard sample; (h) PDSD, recorded on a 2-^{13}C-glycerol-grown checkerboard sample; and (i) PAR, recorded on a uniformly $^{13}C-^{15}N$ labeled sample. Green, red, and blue crosses represent short-range (between residue i and j, $|i - j| < 2$), register ($|i - j| = 35$, 36, or 37), and other medium- or long-range restraints, respectively. Full views with assignments are shown in Supporting Information Figures S3−S12.

were interpreted as $^{13}C-^{13}C$ distances. Restraints from PAIN spectra[51] were interpreted as $^{13}C-^{15}N$ distances.

Structure Calculation. For the structure calculation of the HET-s(218−289) amyloid fibrils, dihedral angle restraints, distance restraints, symmetry restraints, and H-bonding restraints (in the last refinement step only) were used as detailed below. For the dihedral angle restraints, the extended assignment described above was used to generate a list of 82 dihedral angle restraints using the software TALOS.[52] Upper distance restraints were extracted from the nine spectra shown in Figure 3, and their number is listed in Table 1. For each spectrum, all peaks were picked automatically using the CARA software.[53] Clearly recognizable peak shoulders not picked by the automatic procedure were added. Crowded regions (unresolved broader features) were evenly covered with individual peaks spaced by about 0.3 ppm in both dimensions to ensure that all intensities in the spectra are considered in the refinement steps. Peaks arising from the diagonal and spinning sidebands were excluded manually from the peak lists. Ambiguous-distance-restraint (ADR) lists in CYANA format were generated from these peak lists using the chemical-shift values of all assigned residues, a chemical-shift tolerance (see Table 1), and the type of information contained in the spectra according to the experiment and the sample used ($^{13}C-^{13}C$ or $^{1}H-^{1}H$ or $^{13}C-^{15}N$ distances). Except for PDSD spectra, two peak intensity classes were used per spectrum (Table 1). The two classes for each experiment were chosen such that both contain approximately the same number of peaks. Optimized upper distance limits deduced from each experiment were obtained by systematically changing the corresponding value for each restraint class and experiment in steps of 0.5 Å and evaluating the energy target function obtained from CYANA. The resulting L-shaped curves (Figure 4) show that, as expected, the target energy increases very slowly with decreasing distance limits for long trial upper-distance limits. At a certain value, however, the upper-distance limit becomes shorter than the experimental distances accessible by the corresponding experiment and the number of violated experimental restraints increases dramatically, leading to a steep increase of the target energy. We selected the upper distance

(49) Szeverenyi, N. M.; Sullivan, M. J.; Maciel, G. E. *J. Magn. Reson.* **1982**, *47*, 462.
(50) Takegoshi, K.; Nakamura, S.; Terao, T. *Chem. Phys. Lett.* **2001**, *344*, 631.
(51) Lewandowski, J.; DePaepe, G.; Griffin, R. G. *J. Am. Chem. Soc.* **2007**, *129*, 728.
(52) Cornilescu, G.; Delaglio, F.; Bax, A. *J. Biomol. NMR* **1999**, *13*, 289.
(53) Keller, R. *The Computer Aided Resonance Assignment Tutorial*; Cantina Verlag: Goldau, Switzerland, 2004 (see also http://www.nmr.ch).

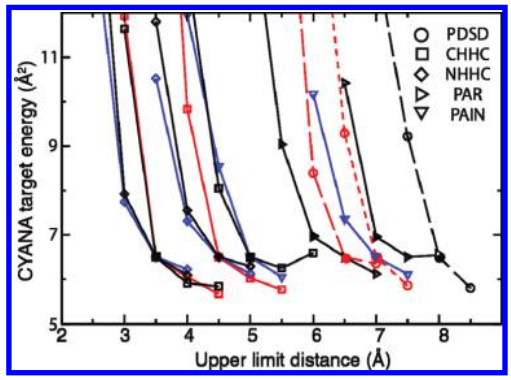

Figure 4. Calibration of the upper limit distance restraints. The CYANA target energy is shown as a function of the upper limit distance of the corresponding structure calculation. The upper limit distance was changed independently for each restraint class in steps of 0.5 Å, and the CYANA target function was averaged for the 10 lowest energy structures (out of 200 calculated structures). The different symbols and colors show the restraint class for which the upper limit distance was changed. The results concerning spectra recorded on homogeneous, diluted, and mixed samples are depicted in black, red, and blue, respectively. Lines for uniformly labeled samples are continuous; those for glycerol labeled samples are dashed (2-^{13}C-glycerol, long; 1,3-^{13}C-glycerol, short). Two intensity classes were used for CHHC, NHHC, and PAR spectra (see text). The distance restraints chosen for the final structure calculation are indicated by filled symbols and are listed in Table 1.

restraint for a certain class of peaks to be the last trial distance (coming from larger values), for which the increase is less than 0.7 Å^2 for a −0.5 Å step. Limits obtained by this procedure are marked by solid symbols in Figure 4 and are given in Table 1. They were used as upper limit restraints in subsequent calculations.

Using the assignment procedure described above, we obtained an average spectral ambiguity per peak of around 10 possibilities (all spectra). Furthermore, the effective number of ambiguities in the structure calculation has to be multiplied by three for restraints extracted from spectra recorded on homogeneously labeled samples, and by two for restraints extracted from spectra recorded on mixed labeled samples, to account for intra- and intermolecular ambiguities.

An analysis of the ambiguous distance restraints already reveals three dominating structural features of HET-s(218−289) (Figure 5). The most eye-catching one concerns the numerous $i/i + 36$ correlations that define the intra- and intermolecular parallel in-register β-sheets. This observation already rules out the models (b), (c), and (d) of Figure 1. Nevertheless, the structure calculation strategy described in the following keeps these possibilities still open.

We first performed a calculation using the TALOS dihedral angle restraints, ADRs from all 15 experiments (see Table 1), and the symmetry restraints on the backbone torsion angles. Three molecules were taken into account, but calculations with up to nine molecules yield a very similar structure for the single HET-s(218−289) molecules. The structure obtained was then used to exclude all assignment possibilities for which the distance was found to be 1.2 times larger than the corresponding upper limit (given in Table 1) in all of the 10 lowest energy structures. As the first run converges unambiguously to a parallel β-sheet structure, the arrangements of Figure 1c and d were now excluded, and additional interface symmetry restraints were added. Also, backbone β-sheet hydrogen bonds were added to the final structure calculation for residues that fulfilled all of the following conditions (see Supporting Information Figure S2):

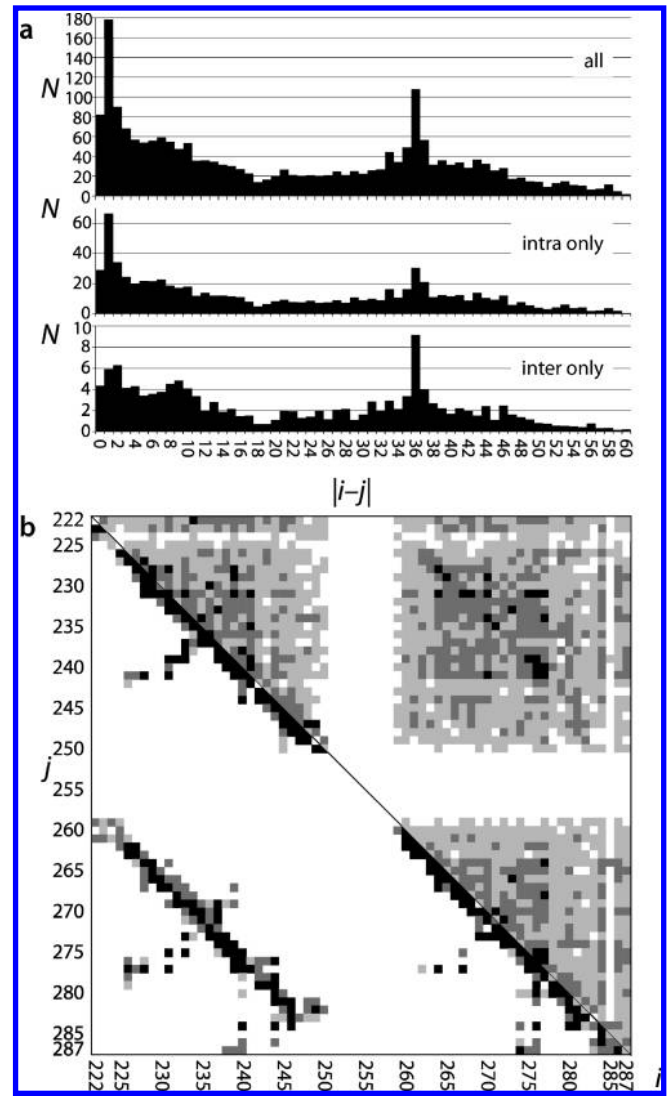

Figure 5. (a) Distance histogram of all ambiguous distance restraints used for the first run of structure calculation. The number N of restraints between residues i and j is counted for each possible distance $|i - j|$, where each ambiguity contributes the inverse of the number of possible assignments for the given restraint (i.e., the contribution of each peak is equal to 1). The sharp peak around $|i - j| = 36$ evidences the existence of the parallel β-sheets in both the intra- and intermolecular stacking. Note that intraresidual heavy-atom correlations were not used in the calculations. (b) Residue−residue plot with black, dark gray, and light gray squares indicating pairs of residues connected at least by 3, 1, and >0.1 "equivalent distance restraints", respectively, where an "equivalent distance restraint" is the sum of distance restraints involving both residues weighted by the inverse of the number of assignment possibilities of the underlying peaks. In the upper right half, all distance restraint ambiguities used for the first run of structure calculation are shown, whereas the lower left part shows all assignment possibilities which were left for the final structure calculation.

(i) their H/D exchange rate was found to be low ($k_{ex} < 0.1$ h^{-1}),[11] (ii) β-sheet secondary structure is predicted by TALOS for both interacting residues, and (iii) the distance between the backbone amide proton and the corresponding H-bonded carbonyl oxygen was less than 3 Å in the 10 lowest energy structures. These additional restraints allow a faster convergence of the structure calculation as well as a better definition of the final structure. The contact plot for the assigned restraints is shown in Figure 5b in the lower triangle. Table 2 shows the statistics for the restraints found in the spectra recorded on the different types of samples. For spectra recorded on homogeneously labeled

Table 2. Assigned Distance Restraints from the Different Spectra and Samples[a]

		no. of fulfilled restraints (unambiguous)[b]			short-range, $\|i-j\| \le 1$[c]		β-sheet, $35 \le \|i-j\| \le 37$		other long- and medium-range, $2 \le \|i-j\| \le 34$ and $38 \le \|i-j\|$	
sample type	spectra	total	intra	inter	intra	inter	intra	inter	intra	inter
diluted	2-^{13}C PDSD	341[c] (39)	341[c] (39)		124[c]		98		119	
	1,3-^{13}C PDSD	428[c] (35)	428[c] (35)		95[c]		113		220	
	U-^{13}C^{15}N CHHC	627 (46)	627 (46)		269		141		217	
mixed	^{15}N/^{13}C NHHC	68 (4)		68 (4)		2		48		18
	^{15}N/^{13}C PAIN	362 (20)		362 (20)		27		158		177
homogeneous	2-^{13}C PDSD	2903[c] (36)	1648[c] (36)	1255 (0)	339[c]	264	343	342	966	649
	U-^{13}C^{15}N PAR	669[c] (7)	415[c] (7)	254 (0)	73[c]	7	127	131	215	116
	U-^{13}C^{15}N NHHC	474 (72)	338 (67)	136 (5)	202	9	84	82	52	45
	U-^{13}C^{15}N CHHC	1213 (44)	764 (43)	449 (1)	257	200	308	75	199	174
total		7085	4561	2524	1359	509	1214	836	1988	1179

[a] All restraints, which are fulfilled within an error of 10% in at least 10 of the 20 lowest energy structures, are listed. They are also mapped onto the fibril structure in Supporting Information Figures S3−S12. [b] Spectrally unambiguous restraints. Note that, for the homogeneously labeled samples, the ambiguity intermolecular/intramolecular remains for most of the peaks. [c] For PDSD and PAR spectra, the observed intraresidue correlations were not used for the structure calculation and are not included in the statistics.

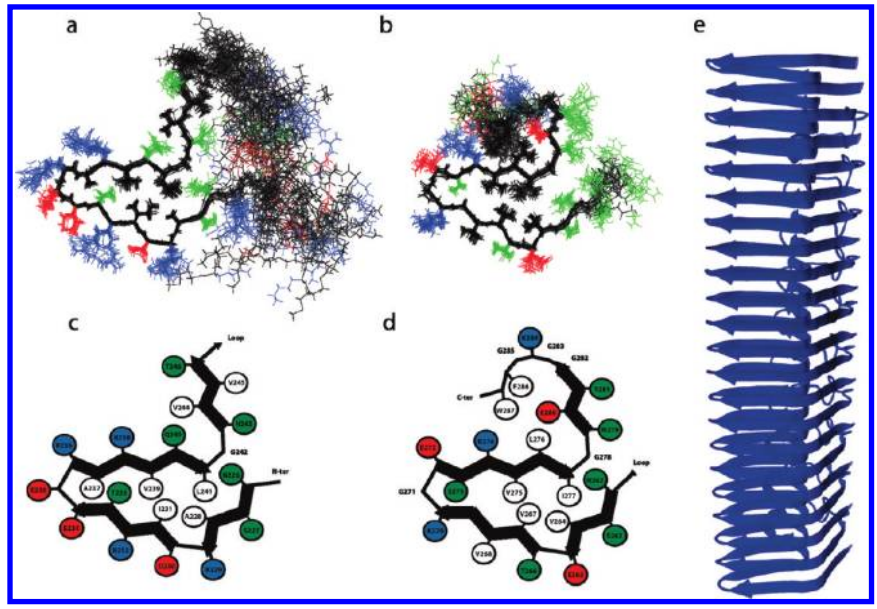

Figure 6. HET-s(218−289) structure. The 20 lowest energy structures (from 200 calculated structures) are superimposed after water refinement in CNS. NMR ensemble of (a) residues K218−S257 superimposed on N226−T246 and (b) residues D258−N289 superimposed on N262-G282. Schematic representations are shown in (c) of the first (N226-T246) and in (d) of the second (N262−W287) β-solenoid layer. Charged residues are displayed in red and blue, polar ones in green, and hydrophobic ones in white. In (e), the stacking in the fibril is shown. The middle molecule for the trimer calculated is translated along the z-axis using a twist of 1.8° per monomer leading to a π rotation over approximately 100 monomers.

samples, the medium- and long-range restraints are almost equally distributed between intra- and intermolecular restraints.

In the final refinement step in water using CNS, the upper limit distance restraints were increased by 10%. The 20 resulting structures representing the NMR ensemble are shown in Figure 6a and b, and they were deposited in the PDB under the accession code 2KJ3. This HET-s(218−289) structure has a backbone/heavy atom rmsd of 0.64/1.00 Å for the residues of the core (N226−T246, N262−G282) and of 1.63/2.34 Å for all assigned residues (I222−A249, T260−W287). The final statistics after refinement in water are given in Table 3. Virtually all observed peaks in the spectra used for the structure calculation can be explained by the obtained structure (Figure 3 and Supporting Information Figures S3−S12), and no evidence for interfibrillar contacts was observed. This confirms the results of the mass-per-length measurements, according to which one HET-s(218−289) molecule forms two layers of β-strands (as displayed in Figure 1). It also indicates that indeed no close

Table 3. Final Statistics after Water Refinement

structure calculation statistics[a]	lowest energy structure	20 lowest energy
residual distance restraint violations > 0.5 Å	0	0
residual dihedral angle restraint violations > 5°	0	1(max7°)
residual van der Waals violations > 0.2 Å	0	0

Ramachandran analysis[b]	core/all assigned/all residues
most favored regions	87.0/87.1/74.9
additional allowed regions	11.0/10.3/19.7
generously allowed regions	0.8/1.2/2.8
disallowed regions	1.2/1.4/2.6

average pairwise rmsd[c]	backbone heavy atoms (Å)	all heavy atoms (Å)
core N226−T246, N262−G282	0.64 ± 0.15/1.00 ± 0.36	1.43 ± 0.17/1.66 ± 0.30
all assigned	1.63 ± 0.55/2.34 ± 0.45	2.34 ± 0.45/2.57 ± 0.48

[a] Structure calculation statistics where the average numbers of violations are given. [b] Results of the Ramachandran analysis of the central molecule for the non-Gly residues of HET-s(218−289) by Procheck NMR.[54] The statistics are given in % as a mean value for the core (N226−T246, N262−G282), for all assigned residues (I222−A249, T260−W287), and for all residues. [c] Average pair-wise rmsd calculated for the central molecule and the three consecutive molecules, respectively. All averages were performed for the 20 lowest energy HET-s(218−289) structures out of a total of 200 structures calculated with CYANA, after CNS water refinement.

interprotofibrillar contacts exist, which is also highly likely considering that the outer interface of the fibrils predominantly consists of hydrophilic residues.

Analysis of the Structural Information Content of Each Spectrum. To better understand what kind of information a specific sample or spectrum contributes, we analyzed the information content of each spectrum (Table 2) and compared structures from calculations including or excluding data derived from one or more spectra. The structure calculations performed using subsets of the experimental data give additional insight in the information needed to obtain specific structural features of the amyloid fibrils (Table 4).

From the data, it becomes clear that spectra recorded on both diluted and mixed samples are necessary to obtain a good convergence of the structure calculation. The data from the homogeneous sample greatly improve the rmsd of the structure obtained. Using solely data extracted from spectra recorded on homogeneously labeled samples, however, leads to the divergence of the structure calculation (Table 4, calculation 9). Only data from diluted, or those from diluted combined with homogeneous samples, allow one to identify the intramolecular β-sheets, whereas data recorded on mixed, or mixed combined with homogeneous, samples allow one to define the intermolecular interface (Table 4, calculations 4−7). Using the data from spectra recorded on diluted and mixed samples only indeed allows the definition of both β-sheet interfaces, the different turns and β-arcs, as well as the hydrophobic core (Table 4, calculation 8). However, the fold of the C-terminus is not as well-defined in this calculation. The addition of data recorded on homogeneous samples, for which a better signal-to-noise is observed, allows one to improve the rmsd of the hydrophobic core and to obtain additional restraints throughout the protein. These data are of importance for the C-terminal part, in particular for the aromatic residues F286 and W287, which are otherwise not restrained. Only the combination of all three types of data is sufficient to fully define the fibril structure.

The comparison of the results of Table 4 also shows that the N−C (NHHC and PAIN) data are especially efficient in identifying β-sheet register contacts, whereas distances extracted from C−C (PDSD or PAR) or CHHC spectra are required to define the hydrophobic core of the protein. This is in line with the statistics shown in Table 3 and Figure 5: most of the long-range distances are found between residue i and j with $35 \leq |i - j| \leq 37$ for NHHC and PAIN spectra, whereas CHHC, PAR, and PDSD spectra contain more other long-range restraints, in particular contacts between side-chains. The use of restraints extracted from PDSD spectra recorded on 2- and 1,3-^{13}C-glycerol-grown samples[21] is beneficial to obtain a better definition of the fold of the protein (Table 4, calculations 2 and 15).

Obtaining the correct handedness of the fibril is most demanding with respect to the quality of the data: a right-handed solenoid and a left-handed solenoid (Figure 7**a**) are practically indistinguishable with respect to C−C and N−C distances. The difference between a left- and right-handed solenoid is reflected by the two possible relative orientations of the two levels of β-sheets in one molecule. For a left-handed solenoid, the winding formed by residues 226−242 followed by winding 262−276 form a left-handed solenoid. For a right-handed solenoid, this order is reversed, leading to the commutation of intermolecular and intramolecular hydrogen bonds in the β-sheets. Therefore, measuring short intermolecular H^N-H^α distances (obtained with the NHHC spectrum recorded on a mixed sample) allows determination of the handedness of the fibrils, as shown in Figure 7b, where the distances d1 and d2 are clearly distinguishable in proton−proton polarization transfer experiments. Accordingly, structure calculations without the "intermolecular" NHHC spectrum always converge to two classes of structures that are similar in all features except handedness. In contrast, a single handedness is only found in calculations containing these NHHC data if the upper limit value is chosen properly for the two distance classes (see Table 4, calculations 16 and 17).

Discussion

The structure (2KJ3) determined here from a large number of restraints, including a high number of spectrally ambiguous ones, shows all features of our previously published structure (2RNM) for the core, as determined from the subset of spectrally unambiguous restraints[14] and extends it to further important residues. The average pairwise rmsd between the two sets of structures (2RNM vs 2KJ3) is 1.28/2.80 Å for the backbone/heavy atom of the rigid core, respectively. The extended structure confirms that six β-arcs, two salt bridges, and three asparagine ladders are present in a left-handed β-solenoid core arrangement (Figure 6). Most of the charged and polar residues are pointing outside the fibril, whereas a patch of hydrophobic residues is protected from solvent in the center of the molecular assembly (Figure 6c and d). The new structure significantly improves the definition of the C-terminal part of the protein. The β-strands β2b and β4b are well-defined (N243−T246 and N279−G282, respectively), and a hydrophobic pocket, which can be looked at as an extension of the hydrophobic core, is revealed (Figure 6). This pocket contains four hydrophobic (V244, L276, F286, and W287) and two charged or polar

(54) Laskowski, R.; Rullmann, J.; MacArthur, M.; Kaptein, R.; Thornton, J. *J. Biomol. NMR* **1996**, *8*, 477.

Table 4. Statistics for Structure Calculations Using Different Subsets of Upper Limit Distance Restraints[a]

		input data								
sample type	spectra	1. all dist H-bonds	2. all dist.	3. no dist.	4. only intra	5. no inter	6. no intra	7. only inter	8. no homog.	9. only homog.
diluted	2-^{13}C PDSD	*	*		*	*			*	
	1,3-^{13}C PDSD	*	*		*	*			*	
	U-^{13}C^{15}N CHHC	*	*		*	*			*	
mixed	^{15}N/^{13}C NHHC	*	*				*	*	*	
	^{15}N/^{13}C PAIN	*	*				*	*	*	
homogeneous	2-^{13}C PDSD	*	*			*	*			*
	U-^{13}C^{15}N PAR	*	*			*	*			*
	U-^{13}C^{15}N NHHC	*	*			*	*			*
	U-^{13}C^{15}N CHHC	*	*			*	*			*
TALOS, symmetry, H-bonds[b]		y all y	y m n	y m n	y m n	y m n	y m n	y m n	y m n	y m n
		results								
rmsd (Å)[c]										
20 lowest energy, 1 molecule		1.16	2.94	6.33	8.26	4.89	15.44	21.61	6.58	19.36
6 lowest energy, left handedness: 1 molecule		1.15	2.95	4.95	7.56	3.70	13.13	15.25	3.41	9.78
6 lowest energy, left handedness: 2 consecutive molecules		1.21	3.03	43.23	38.80	18.60	20.94	22.76	3.49	19.27
Cyana target energy		4	3	0	0	24	14	2	2	9
(lowest/average, a.u.)		5	11	0	1	35	27	5	8	26
structural features[d]		OK	OK	NO	some	some	some	some	some	some
(a) intra/inter register contacts		y y	y y	n n	y n	y n	n y	n y	y y	n y
(b) turns: $\beta1-\beta2$, $\beta3-\beta4$		y	y	n	y	y	y	y	y	y
(c) kinks: $\beta1$ & $\beta3$, $\beta2$ & $\beta4$		y y	y y	n n	y y	y y	y y	n n	y y	y y
(d) folding C-ter		y	y	n	n	y	y	n	n	y
(e) handedness		y	y	n	n	n	y	n	y	n

		input data								
sample type	spectra	10. only NHHC	11. no NHHC	12. NHHC & CHHC	13. no NHHC CHHC	14. inter & PDSD	15. no ext. label	16. inter & fully label	17. all dist. large	18. NHHC inter large
diluted	2-^{13}C PDSD		*		*	*			* + 1 Å	*
	1,3-^{13}C PDSD		*		*	*			* + 1 Å	*
	U-^{13}C^{15}N CHHC		*	*			*		* + 1 Å	*
mixed	^{15}N/^{13}C NHHC	*		*		*	*	*	* + 1 Å	* + 1 Å
	^{15}N/^{13}C PAIN		*		*	*	*	*	* + 1 Å	*
homogeneous	2-^{13}C PDSD		*		*	*			* + 1 Å	*
	U-^{13}C^{15}N PAR		*		*		*	*	* + 1 Å	*
	U-^{13}C^{15}N NHHC	*		*			*	*	* + 1 Å	*
	U-^{13}C^{15}N CHHC		*	*			*	*	* + 1 Å	*
TALOS, symmetry, H-bonds[b]		y m n	y m n	y m n	y m n	y m n	y m n	y m n	y m n	y m n
		results								
rmsd (Å)[c]										
20 lowest energy, 1 molecule		24.95	5.02	12.47	5.39	6.12	8.71	16.69	6.78	4.42
6 lowest energy, left handedness: 1 molecule		24.58	2.33	9.81	2.46	4.10	6.26	14.93	5.39	2.99
6 lowest energy, left handedness: 2 consecutive molecules		40.25	2.46	11.75	2.69	4.38	7.30	19.99	5.66	3.19
Cyana target energy		7	2	29	0	1	12	13	0	3
(lowest/average, a.u.)		14	3	58	1	6	28	28	0	12
structural features[d]		some	some	some	some	OK	some	some	some	some
(a) intra/inter register contacts		n y	y y	y y	y y	y y	y y	n y	y y	y y
(b) arc: $\beta1-\beta2$, $\beta3-\beta4$		n	y	y	y	y	y	y	y	y
(c) arcs: $\beta1$ & $\beta3$, $\beta2$ & $\beta4$		n n	y y	y n	y y	y y	y y	y y	y y	y y
(d) folding C-ter		n	y	n	y	y	n	n	y	y
(e) handedness		n	n	n	n	y	y	n	n	n

[a] For each calculation, 200 structures were computed using CYANA, and the 20 lowest energy structures were analyzed. Input for the structure calculation: For classes marked with an asterisk, the same upper limit distance restraint lists have been used as in the final structure calculations (see Table 2), except for structure calculation number 17 and 18, for which some distances have been increased by 1 Å. [b] The structure calculation is done in the presence (y) or absence (n) of TALOS and H-bond restraints as described in the text. Either a minimal set of symmetry restraints were used (m), which only imposes the different monomers to be in the same conformation (Φ and Ψ angle restraints, see text), or "all" symmetry restraints, including additionally symmetric interfaces, were implemented. [c] The pairwise backbone rmsd was calculated for all assigned residues (I222−A249, T260−W287) of the central molecule or of two neighboring molecules, averaged on the 20 lowest energy structures or on the 6 lowest energy structures belonging to the left handedness family. [d] This rmsd is complemented by the description of the presence or absence of specific structural features. "OK" means that the obtained fold is similar to the best-defined one (obtained with all distance restraints), "NO" and "some" that none or only a few of the characteristic features of the amyloid fibrils are found, respectively. The following list describes in detail whether the characteristic structural features are found (y) or not (n): (a) whether the obtained structure contains the good register pattern for intra- and intermolecular contacts, (b) whether the three-residue arcs between $\beta1$ and $\beta2$, and between $\beta3$ and $\beta4$ are correctly obtained, (c) whether the arcs observed in $\beta1$ and $\beta3$, $\beta2$ and $\beta4$ are present, respectively, (d) whether the C-terminal part, and in particular F286 and W287, fold onto $\beta2$-$\beta4$, and (e) whether the left-handedness of the structure is obtained unambiguously.

residues (Q240 and E280). The E280 side-chain could establish intramolecular hydrogen bonds to G283 NH and G285 C′. The aromatic rings of F286 and W287 show a slightly tilted orthogonal stacking. As this C-terminal entity is required for

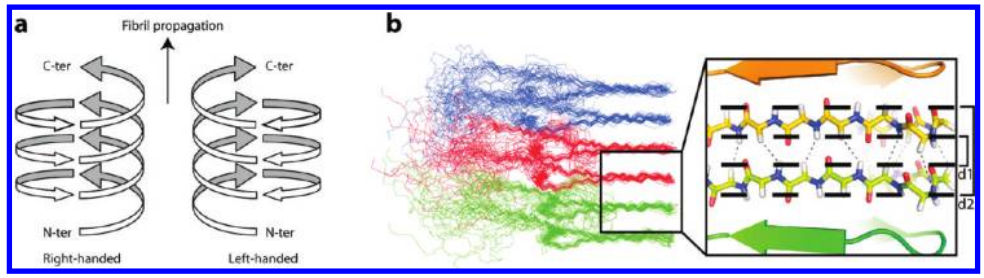

Figure 7. (a) Models for right-handed and left-handed β-solenoids. (b) Backbone side view of three consecutive molecules (bundle of the 20 lowest energy structures) and stick representation of the intermolecular interface of two consecutive HET-s(218−289) molecules in the fibril. The short intermolecular H^N-H^α distances are displayed as dashed lines. The distances d1 and d2 (approximately corresponding to H^N-H^α distances between two consecutive β-sheet layers) are about 2.7 and 7.5 Å, respectively.

HET-s prion propagation (S. Saupe, personal communication), we suggest that this well-organized region may be instrumental for fibril propagation. The aromatic residues F286 and W287 are positioned such that they extend the hydrophobic core of the fibril (Figure 6). The NMR lines for these aromatic residues are broader and less intense than most others and are mainly observed in $^{13}C-^{13}C$ PDSD spectra recorded on homogeneously labeled samples, which exhibit a high signal-to-noise ratio. The finding that the structure of the C-terminus is not as well-defined as the one of the hydrophobic core is therefore not a consequence of missing restraints in the structure calculation but is a consequence of static and/or dynamic disorder in this part of the structure. The structure of the C-terminal part is also of great importance for understanding the polymerization properties of HET-s but also for understanding of the toxicity of HET-S. While the presence of HET-s [or HET-s(218−289)] is not toxic to the *Podospora* cells, the combination of HET-s and HET-S leads to cell death if HET-s is in the prion form. It has been speculated that HET-S inhibits the polymerization of HET-s into harmless prion fibrils and leads to the formation of a large number of toxic oligomers.[15,55] The newly characterized C-terminal part of the fibril can be suspected to be involved into this process which is presently under investigation in our laboratory.

Conclusions

We have presented a protocol to obtain the atomic-resolution structure of HET-s(218−289) amyloid fibrils. The presence of narrow NMR lines, the absence of polymorphism, and the fact that all spectra are fully explained by the resulting structure show that the protofilaments do not pack densely in a regular manner and that the formation of larger fibril bundles, as observed by electron microscopy, does not involve close interfibrillar contacts. The protofibril surfaces are probably almost entirely covered by water.

The high-resolution structure of the HET-s(218−289) fibrils defines a larger part of the molecule by including the coordinates of the C-terminal part and has a higher precision than we had previously achieved. The study demonstrates that the combination of data extracted from complementary 2D NMR spectra collected on diluted, homogeneous, and mixed samples is necessary to obtain the high-resolution structure of the HET-s(218−289) amyloid fibril by solid-state NMR.

The C-terminal part of the fibril was structurally defined and shown to interact with the hydrophobic part of the triangular core of the fibril. Because this part is indispensible for fibril formation and most probably involved into the formation of toxic species causing the heterokaryon incompatibility reaction, the structure described lays the structural basis for further studies to unravel the molecular mechanism of the cell-death reaction.

The approach to structure determination developed in this study can also be used for fibrils with geometries other than those of HET-s. In particular, one molecule may form a different number of windings and the β-sheets may be parallel or antiparallel. For fibrils containing several intertwined protofilaments, the protocol can be revised and extended. In all cases, it should be beneficial to obtain low-resolution information about the geometry of the molecular arrangement with other methods, in particular about the number of direct neighbors of each molecule, in order to simplify the structure determination from solid-state NMR data.

Material and Methods

Preparation of Isotope-Labeled HET-s(218−289) Fibrils. Isotopically labeled HET-s(218−289) with a C-terminal His_6 tag was expressed in *E. coli* as described for other HET-s constructs.[15] The bacterial pellets were dissolved and sonicated in 7.5 M guanidine hydrochloride containing 50 mM TRIS·HCl pH 8.0 and 150 mM sodium chloride. The supernatant was cleared by centrifugation for 1 h at 50000*g*. The protein was purified from the supernatant by Ni-affinity chromatography and concentrated to approximately 0.5−1 mM. Fast buffer exchange was performed to 150 mM acetic acid pH 2.5. Immediately thereafter, the pH was adjusted to 7.5 by addition of 3 M TRIS, which caused HET-s(218−289) to aggregate into amyloid fibrils at 25 °C. The fibrils were washed in H_2O and centrifuged into the magic-angle spinning (MAS) rotor at 200000*g*. At no step was the sample dried or lyophilized. Samples of HET-s(218−289) were also produced using 1,3-^{13}C labeled glycerol and 2-^{13}C labeled glycerol as carbon sources.[21,56] For the production of fibrils consisting of mixtures of differently labeled HET-s(218−289) molecules, the according protein fractions were joined under strongly denaturing conditions (7.5 M GuHCl). All other preparation steps were performed identically for all samples.

Solid-State NMR Experiments. Two-dimensional NMR experiments were conducted on 14.1 and 20.0 T (^1H resonance frequency 600 and 850 MHz, respectively) wide-bore instruments (Bruker Biospin, Germany) equipped with 4 mm Chemagnetics and 3.2 mm Bruker triple-resonance (^1H, ^{13}C, ^{15}N) MAS probes, respectively. All experiments were carried out at sample temperatures of 3−7 °C. MAS frequencies of 19 kHz (20.0 T) and 10 kHz (14.1 T) were used unless stated otherwise. High-power proton decoupling (SPINAL64) with rf amplitudes of 90−110 kHz was applied during evolution and detection periods.

(55) Coustou-Linares, V.; Maddelein, M.-L.; Begueret, J.; Saupe, S. *Mol. Microbiol.* **2001**, *42*, 1325.

(56) LeMaster, D.; Kushlan, D. *J. Am. Chem. Soc.* **1996**, *118*, 9255.

(1) Experiments on 2-^{13}C-Glycerol-Grown HET-s(218−289) Diluted in Natural Abundance (NA) HET-s(218−289) (1:2.5). A PDSD spectrum with a mixing time of 250 ms was recorded at 14.1 T (Figure 3f and Supporting Information Figure S3).

(2) Experiments on 1,3-^{13}C-Glycerol-Grown HET-s(218−289) Diluted in NA HET-s(218−289) (1:2.5). A PDSD spectrum with a mixing time of 500 ms was recorded at 20.0 T (Figure 3g and Supporting Information Figure S4).

(3) Experiments on U-[^{13}C, ^{15}N]-HET-s(218−289) Diluted in NA HET-s(218−289) (1:2.5). A CHHC spectrum with a (^{1}H, ^{1}H) mixing time of 200 μs and t_{HC} = 200 μs was recorded at 14.1 T (Figure 3e and Supporting Information Figure S5).

(4) Experiments on a 1:1 Mixture of U-^{13}C-HET-s(218−289) and U-^{15}N-HETs(218−289). An NHHC spectrum with a (^{1}H, ^{1}H) mixing time of 150 μs, t_{HC} = 200 μs, and t_{NH} = 400 μs was recorded at 20.0 T. For this experiment, the MAS frequency was set to 9.5 kHz (Figure 3b and Supporting Information Figure S6).

A PAIN spectrum with a mixing time of 5 ms was recorded at 20.0 T at an MAS frequency of 19 kHz (Figure 3c and Supporting Information Figure S7).

(5) Experiments on 2-^{13}C-Glycerol-Grown HET-s(218−289). A proton-driven spin diffusion (PDSD) scheme employing a longitudinal mixing time of 250 ms was used. The spectrum was recorded at 14.1 T and 13 kHz MAS (Figure 3h and Supporting Information Figures S8 and S9).

(6) Experiments on U-[^{13}C, ^{15}N]-HET-s(218−289). A PAR[45] spectrum with a mixing time of 3 ms was recorded (Figure 3i and Supporting Information Figure S10).

For the indirect detection of (^{1}H, ^{1}H) correlations, a CHHC[47] spectrum with a (^{1}H, ^{1}H) mixing time of 200 μs was recorded at 20.0 T. Short contact times of t_{HC} = 200 μs enclosing the (^{1}H, ^{1}H) transfer step favored polarization transfer within bonded (^{1}H, ^{13}C) pairs only (Figure 3d and Supporting Information Figure S11).

In addition, an NHHC spectrum with a (^{1}H, ^{1}H) mixing time of 150 μs was recorded at 20.0 T. Contact times of t_{HC} = 200 μs and t_{NH} = 400 μs were used (Figure 3a and Supporting Information Figure S12).

All spectra on this fully labeled sample were carried out at 20.0 T and 19 kHz MAS. All NMR spectra were processed in XwinNMR 3.7 or TopSpin 2.0 (Bruker Biospin) and analyzed using Sparky version 3.113 (T. D. Goddard and D. G. Kneller, University of California, San Francisco, CA) or CARA 1.5.[53]

Structure Calculation. The structure calculations were performed on three consecutive HET-s(218−289) molecules connected by 41-residue linkers with the software CYANA.[39] For each calculation, 200 structures were computed, from which the 20 lowest energy structures were further analyzed. The number of cooling steps during the CYANA molecular dynamics procedure was set to 80 000.[57] The final water refinement was performed using CNS[40] via the RECOORD interface (http://www.ebi.ac.uk/msd/NMR/recoord/). The structures were visualized using PyMol (DeLano Scientific LLC) and MolMol 2K.1 (Reto Koradi, Institut für Molekularbiologie and Biophysik, ETH Zurich).

Acknowledgment. Figures 1 and 2 were produced by Quintin N. Meier. We thank Walter Steurer and Peter Güntert for scientific discussions and the Swiss National Science Foundation and the TH-system of the ETH Zurich for financial support. H.V.M. acknowledges a stipend by the European Union (Marie Curie EIF, FP6), and A.L. by the European Molecular Biology Organization (EMBO). This work was supported by the ANR-PCV08_321323 and the CNRS. The bundle of 20 conformers representing the NMR structure is deposited in the PDB database with accession code 2KJ3, assignments in the BMRB database (ID 11064).

Supporting Information Available: HET-s(218−289) amino-acid sequence, schematic view of the 3D structure with restraints used, and all individual spectra and the restraints obtained from them. This material is available free of charge via the Internet at http://pubs.acs.org.

JA104213J

(57) Fossi, M.; Castellani, T.; Nilges, M.; Oschkinat, H.; van Rossum, B. J. *Angew. Chem., Int. Ed.* **2005**, *44*, 6151.